These results agree in form with the results for nonelectrolytes.[6] The important new features for electrolytes are (1) the present approach is considerably improved in simplicity and accuracy over the previous approach; (2) an explicit formula c_2 itself has been obtained here; and (3) the Soret coefficient σ^* obtained in TGTD experiments on electrolyte solutions differs from the Soret coefficient σ obtained in nonelectrolyte mixtures as discussed at the end of section 3.

ESR Study of the Dynamic Molecular Structure of a Reentrant Nematic Liquid Crystal†

Akbar Nayeem and Jack H. Freed*

Baker Laboratory of Chemistry, Cornell University, Ithaca, New York 14853-1301
(Received: January 26, 1989)

ESR studies of anisotropic ordering and molecular dynamics using a variety of spin probes (PD-Tempone, MOTA, P-probe, and CSL) in a reentrant nematic (RN) liquid crystal mixture, 6OCB-8OCB, are described. In order to discern possible differences in the molecular behavior of reentrant mesogens, our results are compared with similar studies in those liquid crystals that, in spite of being structurally similar to 6OCB–8OCB (e.g., 8CB and S2, which exhibit bilayer smectic-A (S_A) phases), do not exhibit reentrant behavior. Such comparisons show the following. (i) The S_A–RN transition is very similar to the (normal) N–S_A transition. (ii) The orientational ordering of P in the S_A and RN phases of 6OCB–8OCB is consistent with more random packing of the chains than is observed in S2. It is suggested that the collective packing of the chains, which enhances the stability of the S_A phase in a normal liquid crystal (e.g., S2), is frustrated in a reentrant nematic liquid crystal. (iii) The ordering of CSL, which packs with the cores, increases smoothly across the N–S_A–RN transitions, showing that the packing of the aromatic cores is not sensitive to these phase transitions. In general, there are no dramatic changes in the dynamics of the probes upon entering the RN phase of 6OCB–8OCB, supporting the belief that the effects driving reentrance are very subtle. However, the reorientational dynamics of the P-probe indicate enhanced packing of the chains in the RN phase.

I. Introduction

The phenomenon of reentrance in liquid crystals, wherein a particular mesophase is observed to appear whether one heats *or* cools the liquid crystal in some given phase, has been studied extensively both by experimental as well as theoretical methods.[1,2] The most intriguing aspect of this phenomenon is that when the liquid crystal is cooled, an apparently *less* ordered phase is formed—an observation that is counterintuitive from a thermodynamic viewpoint. The reentrant thermodynamic phases in these systems are very sensitive to details of the molecular structure; typically, liquid crystalline molecules possessing strongly dipolar heads (e.g., –CN or $-NO_2$) are observed to form reentrant nematic or reentrant smectic phases,[3] in some cases with double or even quadruple reentrance.[4] Furthermore, reentrant nematic behavior has only been noted in those systems in which the smectic phase is of the bilayer type. On the basis of these general observations, a principal objective in most studies involving reentrant phases has been to deduce mechanisms leading to plausible molecular models for reentrant behavior, and this has been done most commonly in terms of structure–property relationships[5,6] or phenomenological theories.[7-9] Detailed studies on the molecular ordering and dynamics in reentrant mesophases, on the other hand, have received less attention.[10-12] The importance of these latter studies lies in that they can probe the changes in dynamic molecular structure of the liquid crystals as they undergo mesomorphic changes, from which one can better infer the nature of reentrant behavior.

The central purpose of this work is to examine the existing models for reentrant behavior in the light of electron spin relaxation studies of spin probes in a reentrant nematic liquid crystal and thereby suggest criteria for discriminating between different mechanisms of reentrance. A detailed study of critical behavior in the (hexyloxy)biphenyl-(octyloxy)biphenyl (6OCB–8OCB) system has been performed using X-ray techniques with a similar view in mind.[13] The emphasis in our work, however, is on the dynamics of solutes of different shapes in the solvent 6OCB–8OCB, which forms a reentrant nematic phase. We consider here how ESR line-shape studies using a variety of probes dissolved in 6OCB–8OCB reflect the dynamic molecular structure of the reentrant nematic phase, how these results may be analyzed and reconciled in terms of known models for reentrant behavior, and what can be said with regard to possible differences and similarities between ordinary nematic and reentrant nematic structures in terms of nematic–smectic-A (N–S_A) and smectic-A–reentrant nematic (S_A–RN) transitions.

Accordingly, we describe here careful line-shape studies of motionally narrowed and slow-motional ESR spectra of three deuterated nitroxide radicals, 2,2,6,6-tetramethyl-4-piperidone *N*-oxide (PD-Tempone), 4-acetamido-2,2,6,6-tetramethylpiperidine *N*-oxide (MOTA), and 2,2,6,6-tetramethyl-4-[[(butyloxy)-

† Supported by NSF Grant No. DMR 8901718 and NIH Grant No. GM-25862.

(1) For a detailed bibliography covering the literature on reentrant liquid crystals for 1977–1984, see: Hinov, H. P. *Mol. Cryst. Liq. Cryst.* **1986**, *136*, 221.
(2) Cladis, P. E. *Mol. Cryst. Liq. Cryst.* **1988**, *165*, 85.
(3) (a) Cladis, P. E. *Phys. Rev. Lett.* **1975**, *35*, 48. (b) Cladis, P. E.; Bogardus, R. E.; Aadsen, D. *Phys. Rev. A* **1978**, *18*, 2292. (c) Suresh, K. A.; Shashidhar, R.; Heppke, G.; Hopf, R. *Mol. Cryst. Liq. Cryst.* **1983**, *99*, 249.
(4) (a) Sigaud, G.; Tinh, N. H.; Hardouin, F.; Gasparoux, H. *Mol. Cryst. Liq. Cryst.* **1981**, *69*, 81. (b) Tinh, N. H.; Destrade, C.; Gasparoux, H. *Mol. Cryst. Liq. Cryst.* **1982**, *72*, 247. (c) Hardouin, F.; Levelut, A. M. *J. Phys. (Les Ulis, Fr.)* **1980**, *41*, 41. (d) Goodby, J. W.; Walton, C. R. *Mol. Cryst. Liq. Cryst.* **1985**, *122*, 219. (e) Fontes, E.; Heiney, P. A.; Halestine, J. L.; Smith, A. B., III, *J. Phys. (Les Ulis, Fr.)* **1986**, *47*, 1533.
(5) Cladis, P. E. *Mol. Cryst. Liq. Cryst.* **1981**, *67*, 177.
(6) deJeu, W. H. *Solid State Commun.* **1982**, *41*, 529.
(7) Longa, L.; deJeu, W. H. *Phys. Rev. A* **1982**, *26*, 1632.
(8) Prost, J. In *Liquid Crystals in One and Two Dimensions*; Helfrich, W., Heppke, G., Eds.; Springer-Verlag: Berlin, 1980; p 125.
(9) Pershan, P. S.; Prost, J. *J. Phys., Lett.* **1979**, *40*, L-27.
(10) Luckhurst, G. R.; Smith, K. J.; Timimi, B. A. *Mol. Cryst. Liq. Cryst.* **1980**, *56*, 315.
(11) Miyajima, S.; Akaba, K.; Chiba, T. *Solid State Commun.* **1984**, *49*, 675.
(12) (a) Dong, R. Y.; Lewis, J. S.; Tomchuk, E.; Bock, E. *Mol. Cryst. Liq. Cryst.* **1985**, *122*, 35. (b) Emsley, J. W.; Luckhurst, G. R.; Parsons, P. J.; Timimi, B. A. *Mol. Phys.* **1985**, *56*, 767.
(13) (a) Kortan, A. R.; Kanel, H. V.; Birgeneau, R. J.; Litster, J. D. *Phys. Rev. Lett.* **1981**, *47*, 1206; (b) *J. Phys. (Les Ulis, Fr.)* **1984**, *45*, 529.

0022-3654/89/2093-6539$01.50/0

acronym	name	structure
PD-Tempone	2,2,6,6-tetramethyl-4-piperidine *N*-oxide (perdeuterated)	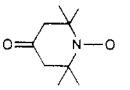
MOTA	4-acetamido-2,2,6,6-tetramethylpiperidine *N*-oxide (perdeuterated ring)	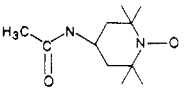
P	2,2,6,6-tetramethyl-4-[[(butyloxy)benzoyl]amino]piperidine *N*-oxide (perdeuterated piperidine ring)	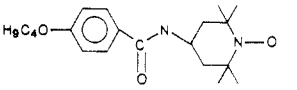
CSL	4,4-dimethylspirooxazolidine-2,3′-5α-cholestane-3-oxy	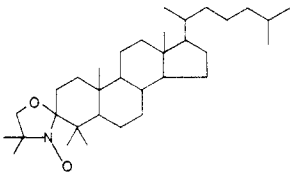

Figure 1. Structures of some spin probes used in this study.

acronym	name	formula
6OCB	4-cyano-4′-(*n*-hexyloxy)biphenyl	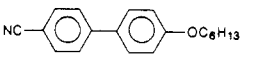
8OCB	4-cyano-4′-(*n*-octyloxy)biphenyl	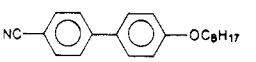
4O,6	*N*-(*p*-butoxybenzylidene)-*p*-*n*-hexylaniline	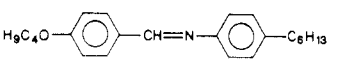
4O,8	*N*-(*p*-butoxybenzylidene)-*p*-*n*-octylaniline	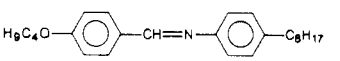
8CB	4-cyano-4′-*n*-octylbiphenyl	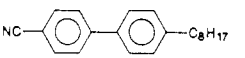
S2	eutectic mixture of	
	50% 4-cyano-4′-*n*-octylbiphenyl,	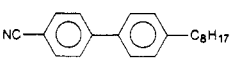
	39% 4-cyano-4′-*n*-decylbiphenyl, and	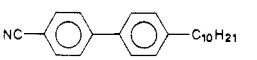
	11% 4-cyano-4′-(*n*-decyloxy)biphenyl	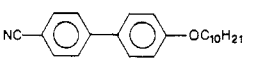

crystals[a]	transition temperature
(a) 27% 6OCB–73% 8OCB	K (24 °C) N (31 °C) S_A (45 °C) N (79 °C) I
(b) 40,6	K (18 °C) S_B (48 °C) S_A (55 °C) N (78 °C) I
(c) 8CB	K (21 °C) S_A (34 °C) N (41 °C) I
(d) S2	K (−10 °C) S_A (48 °C) N (49 °C) I

[a] References: (a) Reference 5. (b) Smith, G. W.; Gardlund, Z. G. *J. Chem. Phys.* **1973**, *59*, 3214. (c) Gray, G. W. *J. Phys.* (*Les Ulis, Fr.*) **1975**, *C-36*, 337. (d) BDH Liquid Crystals Catalog.

Figure 2. Structures of some liquid crystals referred to in this study with their phase transition temperatures.

benzoyl]amino]piperidine *N*-oxide (P-probe), dissolved in a binary mixture of 4-cyano-4′-(hexyloxy)biphenyl (6OCB) and 4-cyano-4′-(octyloxy)biphenyl (8OCB). For compositions of the binary mixture ranging between approximately 25 and 31 wt % 6OCB, this system exhibits a reentrant nematic phase at atmospheric pressure;[5] i.e., one observes a transition from the smectic-A to nematic phase on either heating or cooling the system. The advantage of several probes being used for such a study is that different spin labels are sensitive to different motional time scales owing to their differences in size; furthermore, owing to differences in ordering and their tendency to reside near different parts of the solvent molecules (e.g., aromatic vs aliphatic regions of the liquid crystals), they are useful probes of local changes in structure and dynamics.[14] Thus, from Figure 1, we note that PD-Tempone is a relatively small, quasi-spheroidal probe; it typically exhibits fast motion ($\tau_R \approx 10^{-10}$–10^{-12} s) and low ordering.[15-17] The P-probe is a larger, more liquid-crystal-like molecule that can be expected to show greater changes in ordering and motional effects in response to changes in the mesomorphic environment.[18] MOTA is a molecule that is intermediate in size between PD-Tempone and P. One therefore expects to see a range in ordering and dynamics for these three probes that parallels their differences in size and geometry.

The experimental details of the paper are given in section II. Section III provides a summary of the models that have been proposed to explain reentrance in liquid crystals, highlighting those

(14) (a) Freed, J. H. In *Spin Labeling: Theory and Applications*; Berliner, L. J., Ed.; Academic: New York, 1976; Chapter 3. (b) Freed, J. H. In *Rotational Dynamics of Small and Macromolecules*; Dorfmuller, Th. Pecora, R., Eds.; Springer-Verlag: Berlin, 1987; p 89.

(15) Hwang, J. S.; Mason, R. P.; Hwang, L. P.; Freed, J. H. *J. Phys. Chem.* **1975**, *79*, 489.

(16) (a) Lin, W. J.; Freed, J. H. *J. Phys. Chem.* **1979**, *83*, 379. (b) Meirovitch, E.; Freed, J. H. *J. Phys. Chem.* **1980**, *84*, 2459.

(17) (a) Polnaszek, C. F.; Freed, J. H. *J. Phys. Chem.* **1975**, *79*, 2283. (b) Rao, K. V. S.; Polnaszek, C. F.; Freed, J. H. *J. Phys. Chem.* **1977**, *81*, 449.

(18) (a) Meirovitch, E.; Igner, D.; Igner, E.; Moro, G.; Freed, J. H. *J. Chem. Phys.* **1982**, *77*, 3915. (b) Meirovitch, E. *J. Phys. Chem.* **1984**, *88*, 2863 (in this article, the P-probe carries the acronym TBBP).

aspects that are particularly relevant to our study. Section IV presents first some background material related to the analysis of our data—this includes the choice of magnetic parameters and the calculation of order parameters. This is followed by a discussion of our results on the probe ordering and rotational correlation times in the various mesophases of 6OCB–8OCB, placing special emphasis on the changes at the N–S_A and S_A–RN transitions. Finally, in section V, we provide a discussion of our results in light of current models for reentrant behavior and indicate how our observations with the spin probes may be used to help to discriminate between them. The conclusions are summarized in section VI.

II. Experimental Section

A. Preparation of Samples. The liquid crystals 6OCB and 8OCB, shown in Figure 2, were purchased from BDH Chemicals Ltd. and used without further purification since their phase-transition temperatures were in good agreement with the published values.[5] The required sample consisting of 27.2% 6OCB and 72.8% 8OCB by weight was prepared by weighing sufficient quantities of the components so that the final concentrations were known to within 0.1% by weight.

The molecular structures of the spin probes are shown in Figure 1. PD-Tempone was prepared in these laboratories by standard techniques as discussed by Hwang et al.[15] MOTA was supplied to us by Prof. J. Pilar; its synthesis and use in an earlier ESR study have been described elsewhere.[19] The P-probe was prepared by Sidney Wolfe (University of California, Berkeley) and supplied to us by Prof. Alex Pines.

The spin-probe solutions of approximate concentration 0.2 mM were prepared by degassing the samples (contained in cylindrical Pyrex tubes of internal diameter ≈2 mm) under vacuum and then sealing off under a pressure below 0.1 mTorr.

B. ESR Spectrometer. All ESR measurements were performed on a Varian E-12 spectrometer with 10-kHz field modulation, or 25 kHz when needed. The temperature in the active region of the cavity was controlled by a Varian E-257 variable-temperature control unit to a long-term stability of ±0.5 °C, with dry nitrogen as the medium for heat transfer. The copper–constantan thermocouple junction, which was used for temperature measurements, was placed just over the active microwave region.

C. Aligning the Director. At 3 kG, the external magnetic field is strong enough to align the director in the nematic phase parallel to itself. In order to align the director in the smectic-A phase, however, it is necessary to use a stronger magnetic field.[16] In order to achieve a satisfactory alignment, the field was increased to about 12 kG and the sample temperature gradually lowered (from the nematic state) until the smectic phase was formed. The temperature was then gently raised until the stable nematic phase was formed. This cycle of cooling and heating was repeated a few times at the vicinity of the N–S_A transition. Ultimately, the temperature was lowered until the pure S_A phase was formed. The fact that the director in the smectic phase was well aligned was indicated by the sharpness and symmetry of the ESR lines for the spectra taken at different smectic tilt angles.

D. Line-Width Measurements. All spectral measurements were made on the E-12 spectrometer interfaced to a Prime 850 time-shared computer, with the modulation amplitude set below one-tenth of the peak to peak line width and the microwave power well below the saturation limit. The intrinsic line widths for each of the three hyperfine lines were obtained by fitting each line to a superposition of Lorentzian lines separated by a_D, the deuterium coupling constant.[16,17] Examples of such fits can be found in ref 16a.

In the case of slow-motional spectra, such as those observed in the smectic phase with the P-probe, such a treatment could not be used, owing in part to overlap between the hyperfine lines. In this case, the entire spectrum was simulated in order to obtain the dynamic parameters.[18]

(19) Pilar, J.; Labsky, J.; Kalal, J.; Freed, J. H. *J. Phys. Chem.* **1979**, *83*, 1907.

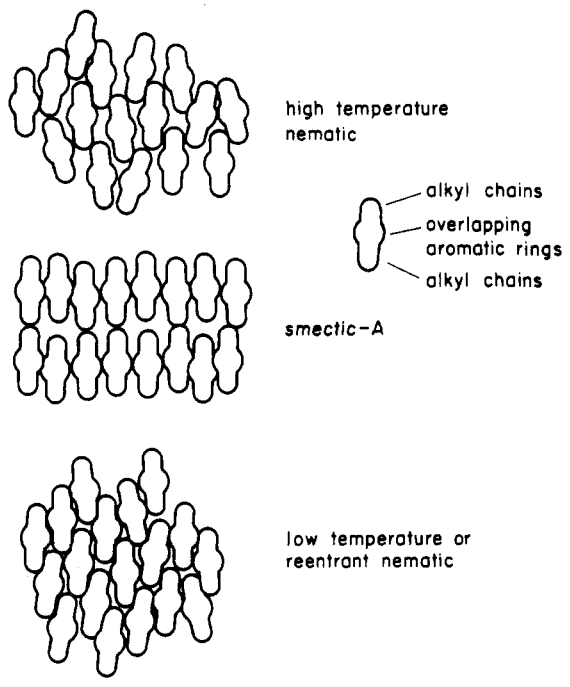

Figure 3. Proposed arrangement of associated dipolar pairs in nematic, smectic-A, and reentrant nematic phases (cf. ref 2 and 3b).

III. Models for Reentrant Behavior

The molecules most commonly observed to exhibit a reentrant nematic phase have been noted to possess a strongly polar group at one end of the molecule (in the case of the cyanobiphenyls, the cyano group for which the dipole moment is 4.5 D) and exhibit a smectic phase in which the interlayer spacing is incommensurate with a single molecular length (usually bilayer or partial bilayer). Although the molecular reason for reentrance is not satisfactorily understood, it is believed to be dependent on the strong antiferromagnetic correlation of the terminal dipoles that results in a bilayer structure for the smectic phase.[3,5] On the basis of pressure and temperature studies, Cladis[3,5] has proposed that as the densities of these substances in the (bilayer) smectic phase increase, a point is reached at which the partial bilayer arrangement of the smectic phase breaks down, leading to an arrangement in which the molecules, paired together as antiparallel dimers, form interdigitated layers with loss of smectic ordering (see Figure 3). Subsequent studies on the variation of density with temperature for three distinct 6OCB–8OCB mixtures by Bouchet and Cladis[20] have shown the densities of these mixtures to vary in a similar way, regardless of whether the system does or does not exhibit an RN phase—showing that if changes in the slope of density vs temperature are due to changes in the number of molecular associations, then such associations must occur independent of reentrance. The initial curvatures of the (isobaric) density versus temperature plots for 6OCB–8OCB were interpreted in terms of the enhanced association between the molecules that occurs as the temperature is lowered. At sufficiently low temperatures in the S_A phase, the observed linear variation of density with temperature was taken to imply a saturation in the formation of such pairs—a point at which most of the molecules exist as dimers. Consequently, smectic bilayers composed of such (associated) molecules possess larger voids in the hydrocarbon regions (Figure 3) than layers composed of molecules that do not tend to associate or those that form smectic layers of the monolayer type. As the temperature of the system is lowered or the pressure raised, the molecules, in attempting to pack more efficiently (increasing the density), rearrange themselves in such a way as to fill these voids, thus destroying the smectic ordering and resulting in the induction of the reentrant nematic phase (provided that crystallization does not occur). In this model, the formation of the dimers is believed

(20) Bouchet, F. R.; Cladis, P. E. *Mol. Cryst. Liq. Cryst.* **1980**, *64*, 81.

to be facilitated by the fact that the molecules are highly polar and can therefore form stable dimers in a way such that oppositely charged ends of the molecules could overlap.[2,3b] The polarity, which enhances molecular association, is therefore regarded as the driving force for reentrance.

The model described above implies that, at some *optimum density*, the forces stabilizing smectic ordering (e.g., long-range electrostatic interactions) are overcome by steric effects that result in more efficient molecular packing. This has been described more quantitatively in terms of Landau mean-field theory by Pershan and Prost.[9] The smectic order parameter $|\Psi|$ is assumed to couple to the density (and composition in the case of binary mixtures). This coupling, which when included in lowest order in the density predicts the correct phase diagram for 8OCB and for 6OCB–8OCB (see ref 9 and 13 and Discussion in section V below), provides a more general description of reentrance than that outlined above. However, the molecular details leading to an increased density are not explicitly addressed. More particularly, a saturation in pair formation is not regarded as a fundamental prerequisite for reentrance. Indeed, a stable reentrant nematic phase has also been reported in a binary mixture of terminal *nonpolar* compounds, and furthermore, X-ray studies on the RN phase in this case indicated no hint of dimerization found in reentrant systems with polar substances.[21] (In this latter study, the residual layer ordering noted in the RN phase was attributed to the existence of cybotactic clusters.) Furthermore, the nonlinearity in density vs temperature observed by Bouchet and Cladis[20] is also characteristic of monolayer smectics.[22]

Reentrant nematic behavior has also been observed in a system found to exhibit the phase-transition sequence N–S_A–N–S_A, where the high-temperature S_A is of the bilayer type and the low-temperature S_A is of the monolayer type.[4c] The intermediate phase, the reentrant nematic, has therefore also been regarded as formed owing to the competition between two local S_A orders, one favoring the formation of bilayers and the other the formation of monolayers.[4c,23] However, much support for this has not been available.

In addition to phenomenological theories, molecular theories have also been invoked to describe reentrant behavior. Dowell, using a lattice model for bulk phases of molecules having only hard repulsions,[24] shows that owing to differences in packing between rigid cores and semiflexible tails (representing, respectively, the aromatic rings and the alkyl chain ends of the liquid crystal molecules), a range of temperatures and/or pressures can be found in which the molecules are arranged in a manner such that the cores tend to pack with cores and the tails tend to pack with tails. This arrangement corresponds to a stable S_A phase. According to the model, as the temperature is reduced (and/or the pressure is increased), the tails become more rigid and rodlike, thus reducing the advantage of packing cores with cores and tails with tails. At some optimum point in temperature, the S_A phase thus disappears, allowing the nematic phase to reappear at a lower temperature.

There are two particularly interesting features of Dowell's steric packing model that are germane to our study. Firstly, since dipolar interactions are not considered to be *necessary* for the formation of stable S_A and reentrant nematic phases (although they affect the range of temperatures and pressures over which the S_A and RN phases are stable), (i) a pairing mechanism is not necessary to account for reentrance and (ii) the ordinary (high-temperature) nematic is fundamentally similar to the reentrant (low-temperature) nematic (as they should be since they really are the same phase). Both of these statements are supported by the fact that (a) the X-ray results of Kortan et al.[13] show no evidence in support of enhanced pairing in the RN phase (unless it is very gentle) and (b) the reentrant behavior is observed in mixtures of terminally nonpolar compounds[21] where there is little tendency for the molecules to associate. Secondly, Dowell's observations on the way in which the packing forces stabilize the S_A phase in a pure compound can be used to speculate on how solute molecules of different shapes might affect the stability of the S_A phase. In general, Dowell proposes[24] that the more flexible solutes probably associate with the solvent chain regions and the more rigid, rodlike solutes reside near the solvent rigid cores. In addition, relatively globular, quasi-spherical solutes are expected to pack with the solvent tail chains in order to minimize the reduction in orientational ordering of the cores. Although such predictions would, of course, be modified when attractive forces are included, they nevertheless suggest that when external solutes are used as probes of the orientational ordering and dynamics of liquid crystals exhibiting a S_A phase, the structure of the solute will influence which parts of the liquid crystal are being probed. Indeed, the various spin probes used in this study of 6OCB–8OCB show distinct differences in their ordering and spin relaxation behavior (see text below).

TABLE I: Magnetic Parameters for Spin Probes in 6OCB–8OCB[a]

probe	$g_{x'''}$	$g_{y'''}$	$g_{z'''}$	$A_{x'''}$, G	$A_{y'''}$, G	$A_{z'''}$, G
Pd-Tempone	2.0099	2.0062	2.00215	5.60	5.00	33.65
MOTA	2.0099	2.0064	2.0023	5.92	5.29	35.60
P-probe	2.0094	2.0058	2.0026	7.34	7.84	31.60
CSL	2.0088	2.0058	2.0027	6.48	6.48	34.39

[a] a_N: (i) PD-Tempone, 14.75 G (I phase) and 14.67 G (S_A phase); (ii) MOTA, 15.60 G (I phase) and 15.69 G (S_A phase).

More recently, a microscopic spin-gas model has been used to explain the sequence of reentrant transitions now observed in several liquid crystals.[25] The frustration in a smectic system of dipolar molecules is relieved by fluctuations that induce reentrance, implying a competition between short-range positional order and long-range antiferroelectric order. Though this model, when solved in two dimensions, does predict a reentrant phase diagram similar to the one observed, it proposes a mechanism for the S_A–RN transition that is quite different from ordinary N–S_A transitions. Since our studies on critical effects at N–S_A and S_A–RN transitions in 6OCB–8OCB mixtures have not indicated this to be so[26] [nor have the X-ray results of Kortan et al.[13]], the relevance of the spin-gas model to our results seems unclear.

IV. Results and Analysis

A. Magnetic Parameters. A fundamental quantity is a_N, the isotropic hyperfine constant, whose value is sensitive to the polarity of the solvent.[16,17] In the smectic-A phase, a_N is obtained by measuring the average hyperfine splitting $\langle a \rangle$ at different values of θ, the tilt angle between the mean smectic director and the static field, and using the relation

$$\langle a \rangle \approx a_N + \frac{\chi}{2}(3\cos^2\theta - 1)$$

where χ depends on the degree of ordering. a_N is conveniently obtained by measuring $\langle a \rangle$ at $\theta = 0°$ and 90° in the S_A phase, since $\langle a \rangle_{0°} = a_N + \chi$ and $\langle a \rangle_{90°} = a_N - 0.5\chi$. The a_N thus measured at different temperatures in the S_A phase were found to be practically the same (except for the P-probe). a_N in the nematic phase was taken as the mean of the values of a_N in the smectic-A and isotropic phases. Since the lower temperature nematic phase had a narrow temperature range, a_N in the reentrant nematic phase was assumed to be the same as that in the S_A phase.

The components of the hyperfine and **g** tensors for each of the three spin probes (PD-Tempone, MOTA, and P) were obtained by scaling the (measured) a_N and g_S to those measured previously for the same spin probes in similar liquid crystals (see, e.g., ref 18b and 27). This method, which makes use of the linear cor-

(21) Diele, S.; Pelzl, G.; Latif, I.; Demus, D. *Mol. Cryst. Liq. Cryst.* **1983**, *92*, 27.
(22) Rao, N. V. S.; Pisipati, V. G. K. M. *J. Phys. Chem.* **1983**, *87*, 899.
(23) Prost, J.; Barois, P. *J. Chim. Phys. Phys.-Chim. Biol.* **1983**, *80*, 67.
(24) (a) Dowell, F. *Phys. Rev. A* **1983**, *28*, 3526; (b) *Ibid.* **1987**, *36*, 5046.
(25) (a) Berker, A. N.; Walker, J. S. *Phys. Rev. Lett.* **1981**, *47*, 1469. (b) Indekeu, J. O.; Berker, A. N. *Phys. Rev. A* **1986**, *33*, 1158. (c) *J. Phys.* (*Les Ulis, Fr.*) **1988**, *49*, 353.
(26) (a) Nayeem, A. Ph.D. Thesis, Cornell University, 1986. (b) Nayeem, A.; Rananavare, S. B.; Sastry, V. S. S.; Freed, J. H. *Proceedings of the Twelfth International Liquid Crystal Conference*, Berkeley, CA, 1986, and in preparation.

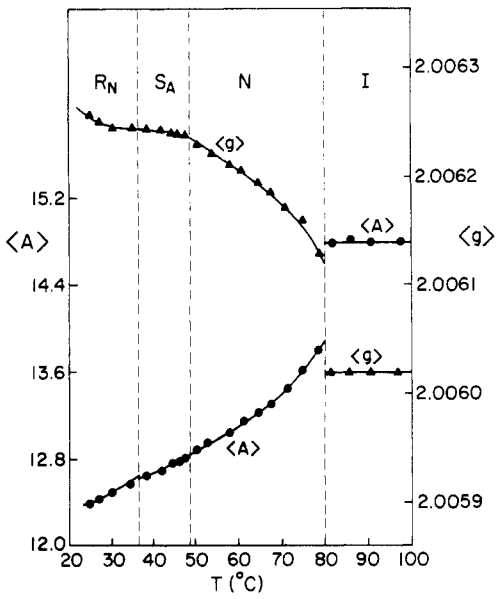

Figure 4. Hyperfine splitting ($\langle a \rangle$, in gauss) and g values ($\langle g \rangle$) for PD-Tempone in 6OCB–8OCB.

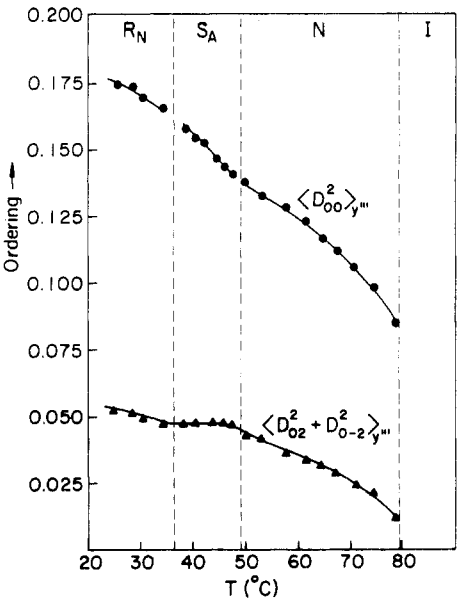

Figure 5. Order parameters for PD-Tempone in 6OCB-8OCB. ($\langle D_{00}^2 \rangle$ and $\langle D_{02}^2 + D_{0-2}^2 \rangle$ are defined in the text.)

relation between the molar transition energy of the solvent (a measure of its polarity) and the hyperfine splitting constants,[16a] has been described elsewhere.[28] The components of the magnetic tensors thus obtained are shown in Table I, together with the values of a_N for PD-Tempone and MOTA in the I and S_A phases.

The value of a_N for PD-Tempone is found to decrease on going from I–N–S_A. This is in agreement with the results for this probe in a variety of other liquid crystalline solvents.[16a] It is interpreted as due to the gradual expulsion of the probe from the polar regions of the solvent to the more nonpolar head groups. However, a_N for MOTA shows the reverse trend. (The values of a_N for P were obtained from line-shape simulations. They are not precise enough to distinguish small variations in a_N with the phase.)

B. Order Parameters and Potential Expansion Coefficients. (*i*) *PD-Tempone in* 6OCB–8OCB. The spectra in all phases consisted of three well-separated hyperfine lines, from which the $\langle a \rangle$ and $\langle g \rangle$ shifts could be directly measured (Figure 4). The values thus measured were corrected for dynamic frequency shifts due to nonsecular terms (since $\tau_R \approx 10^{-11}$ s) and were then used to calculate the two order parameters $\langle D_{00}^2 \rangle$ and $\langle D_{02}^2 + D_{0-2}^2 \rangle$:[16,17]

$$\langle D_{00}^2 \rangle_{y'''} = \frac{(\langle a \rangle - a_N)(g_z - g_x) - (\langle g \rangle - g)(A_z - A_x)}{(A_y - a_N)(g_z - g_x) - (g_y - g)(A_z - A_x)}$$

$$\langle D_{02}^2 + D_{0-2}^2 \rangle_{y'''} = \frac{6^{1/2}[(\langle a \rangle - a_N)(g_y - g) - (\langle g \rangle - g)(A_y - a_N)]}{(A_y - a_N)(g_z - g_x) - (g_y - g)(A_z - A_x)}$$

The subscript y''' on the order parameters denotes that the y-axis of the magnetic frame coincides with the principal (z) axis of ordering (i.e., the z-axis of the diffusion tensor).

The ordering in all phases is low (Figure 5), and the order parameter $\langle D_{00}^2 \rangle$ lies in the same general regime as that for PD-Tempone in 8CB, 4O,6, or 4O.8.[16] It rises steeply as the temperature is lowered below the N–I transition in the nematic phase and appears to connect continuously with $\langle D_{00}^2 \rangle$ in the S_A phase. As noted in a previous study of PD-Tempone in 8CB, the order parameter $\langle D_{00}^2 \rangle$ increases, whereas $\langle D_{02}^2 + D_{0-2}^2 \rangle$, which had increased in the nematic phase, remains practically constant as the temperature is lowered in the S_A phase. As with 8CB, this is interpreted as follows: The tendency of bilayering means that the polar end groups of the liquid crystal molecules tend to draw closer. Whereas this is the basis of the bilayer smectic structure in the *n*CB as well as the *n*OCB homologous series, one may expect short-range order involving such bilayer formation even in the nematic phase. Thus, there should be a preference for the PD-Tempone molecules to reside in the less ordered aliphatic chain regions. The changeover to the smectic phase from the nematic phase is continuous, as expected for a second-order phase transition. As the temperature is lowered in the S_A phase, the aliphatic chains continue to exhibit enhanced ordering but principally along the direction of the nematic director. Furthermore, we note a continuous variation in $\langle D_{00}^2 \rangle$ and $\langle D_{02}^2 + D_{0-2}^2 \rangle$ across the S_A–RN transition, consistent with this also being a second-order transition.

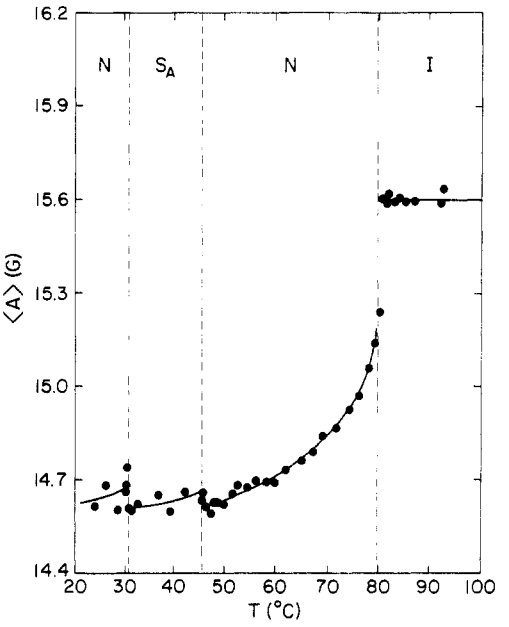

Figure 6. Hyperfine splittings ($\langle a \rangle$) for MOTA in 6OCB–8OCB.

(*ii*) *MOTA in 6OCB–8OCB.* The variation of the measured hyperfine values with temperature is shown in Figure 6. Measurements of $\langle a \rangle$ in the S_A phase at 0° and 90° orientations of the director relative to the static field were used to calculate a_N as described above. The order parameter $\langle D_{00}^2 \rangle$ was calculated as follows:

$$\langle D_{00}^2 \rangle = \frac{\langle a \rangle_{0°} - a_N}{A_z - a_N}$$

(27) Meirovitch, E.; Freed, J. H. *J. Phys. Chem.* **1984**, *88*, 4995.
(28) Zager, S. A.; Freed, J. H. *J. Chem. Phys.* **1982**, *77*, 3344.

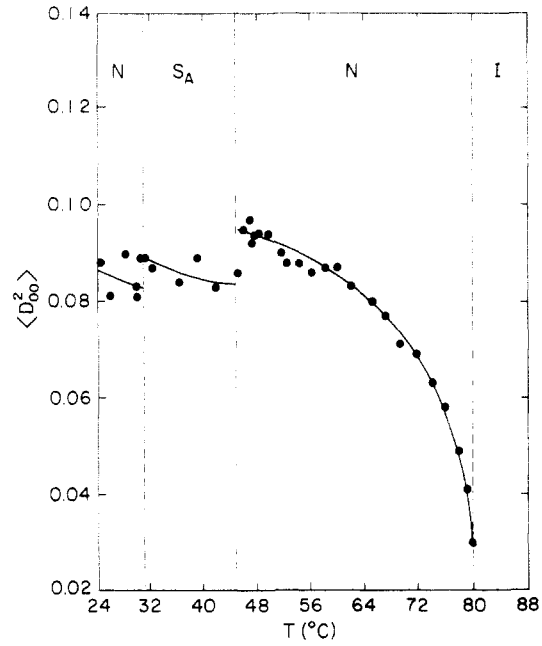

Figure 7. Order parameter $\langle D_{00}^2 \rangle$ for MOTA in 6OCB–8OCB.

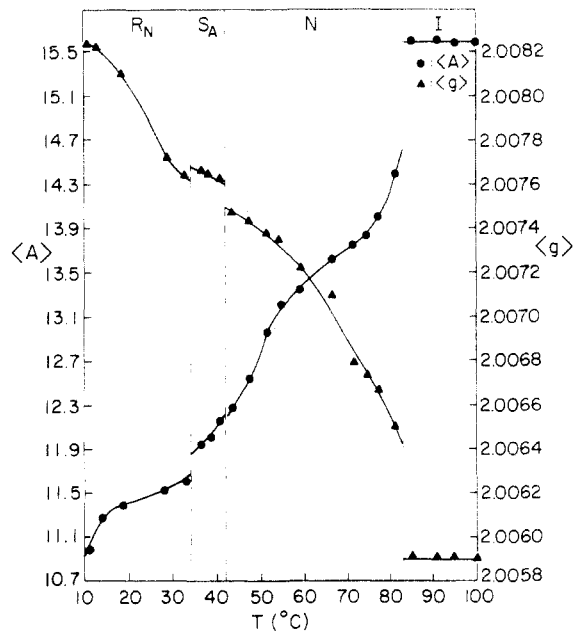

Figure 8. Hyperfine splittings ($\langle a \rangle$, in gauss) and g values ($\langle g \rangle$) for P-probe in 6OCB–8OCB.

Contrary to what we may have expected, the ordering for the larger molecule MOTA (Figure 7) is actually *lower* than for PD-Tempone (compare with Figure 5); this may also be inferred from the relative jumps in the values of $\langle a \rangle$ in passing from the isotropic to the nematic phase in the two cases. It is possible that owing to free rotation about the N–C and C–C bonds in the acetamide moiety in MOTA, a steric resistance is created that inhibits the probe from residing near the cores of the liquid crystals. Indeed, when the S_A phase is reached, $\langle D_{00}^2 \rangle$ decreases, consistent with MOTA being expelled deeper into the aliphatic chain region. No change in the ordering is observed at the transition to the reentrant nematic phase nor within that phase.

(iii) P in 6OCB–8OCB. The spectra of P were found to lie in the incipient slow-motional regime in the ordered phases. Thus, the expressions given above for calculating the order parameters from the observed $\langle a \rangle$ and $\langle g \rangle$ values, shown in Figure 8, are not appropriate here. Therefore, complete line-shape simulations were performed in order to obtain λ and ρ, the two parameters that

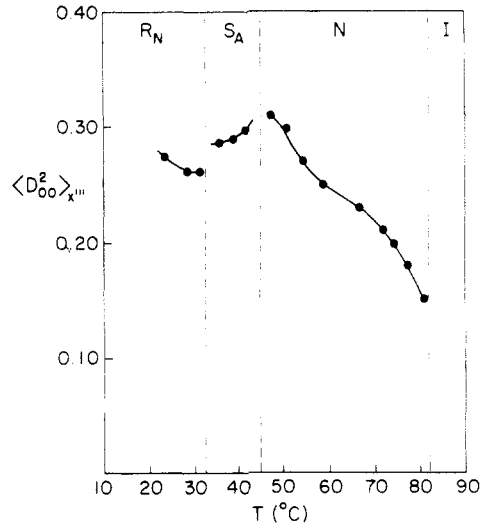

Figure 9. Order parameter for P-probe 6OCB–8OCB as obtained from spectral simulations.

define the ordering potential,[18] and are related to the order parameters as follows:

$$\langle D_{00}^2 \rangle = Z^{-1} \int \tfrac{1}{2}(3\cos^2\beta - 1) e^{[\lambda D_{00}^2(\Omega) + \rho(D_{02}^2(\Omega) + D_{0-2}^2(\Omega))]}\, d\Omega$$

$$\langle D_{02}^2 + D_{0-2}^2 \rangle = Z^{-1} \int (\tfrac{3}{2})^{1/2} \sin^2\beta \cos(2\alpha)\, e^{[\lambda D_{00}^2(\Omega) + \rho(D_{02}^2(\Omega) + D_{0-2}^2(\Omega))]}\, d\Omega$$

where

$$Z = \int e^{[\lambda D_{00}^2(\Omega) + \rho(D_{02}^2(\Omega) + D_{0-2}^2(\Omega))]}\, d\Omega$$

and $d\Omega = d\alpha \sin\beta\, d\beta\, d\gamma$. In these equations, $\Omega(\alpha, \beta, \gamma)$ denotes the set of Euler angles that specify the orientation of the spin probe with respect to the director.

Our line-width data in the isotropic phase were indicative of anisotropic diffusion with $N = 4$ (N defined in text below), and in the ordered phases, the values of N were still higher (see below), indicative of rapid rotational motion about the ordering axis. This suggested that an axially symmetric ordering tensor be used in our simulations. Furthermore, an examination of the structure of the molecule (Figure 1) reveals that the molecule has its primary diffusion axis pointing along the magnetic x (or x''') axis. The magnetic x-axis was therefore chosen as the primary reference axis.

The order parameter $\langle D_{00}^2 \rangle_{x'''}$ is shown as a function of temperature in the different phases in Figure 9. We note that the ordering is low to moderate in these phases. Unlike PD-Tempone, the ordering decreases slightly in the S_A phase. When the liquid crystal is cooled further, the nematic phase reappears and there is a decrease in the ordering. Though the narrow range of the low-temperature nematic phase (≈7 °C) precludes a detailed study, the observation that the ordering decreases and remains practically unchanged in this narrow temperature range is consistent with some expulsion of the P-probe from the central core region. The ordering of P observed here is similar in magnitude to P-probe in S2[18] at comparable temperatures, but no decrease in ordering in the S_A phase was observed for S2.

C. Line-Width Analyses and Motional Dynamics. (i) PD-Tempone. The ESR spectra of PD-Tempone in 6OCB–8OCB fall in the motionally narrowed regime. The dynamics of the spin probe are described in terms of the rotational correlation times and order parameters, obtained from the line-width parameters A–C defined as[15]

$$A = \delta(0)$$

$$B = (\tfrac{1}{2})[\delta(1) - \delta(-1)]$$

$$C = (\tfrac{1}{2})[\delta(1) + \delta(-1) - 2\delta(0)]$$

where the indices +1, 0, and −1 for δ (the intrinsic derivative line widths) refer to the low, middle, and high field lines, respectively.

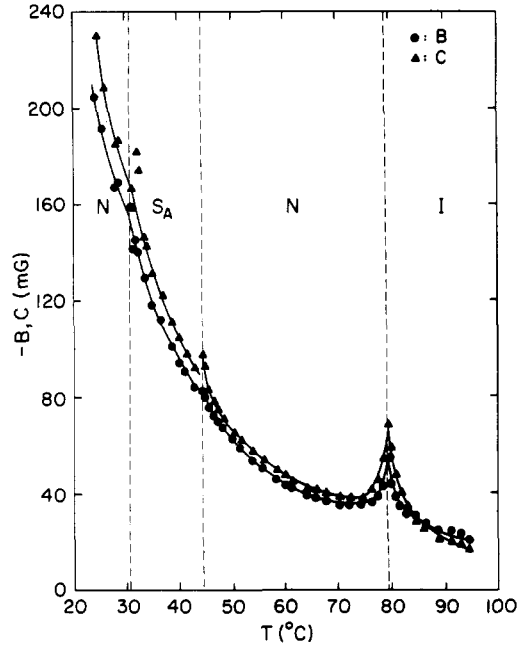

Figure 10. Line-width data (*B* and *C*) for PD-Tempone in 6OCB–8OCB as a function of temperature.

For isotropic liquids, *B* and *C* can be used to obtain the rotational correlation time(s). For ordered liquids, *A*–*C* depend on the ordering as well and the relationship is more complex.[17]

The variation of *B* and *C* with temperature is shown in Figure 10. As in previous studies with PD-Tempone in various solvents,[15-17] we found that *B* and *C* in the isotropic phase were nearly equal. As the nematic phase was approached, *C* increased at a greater rate than *B*, and this anomalous increase in *B* and *C* was also observed as the N–I transition was approached from the nematic side. Such effects are related to order fluctuations at this weakly first-order transition.[26,29] However, since the nematic range is fairly wide (≈35 °C), this effect does not obscure the nonanomalous portions of *B* and *C* in the nematic phase and reliable estimates of the activation energy for reorientation can therefore be made.

The parameters *B* and *C* are interpreted in terms of the rotational dynamics of the probe. An expression for *B* and *C* in isotropic liquids, which includes corrections due to slow motion and modified (non-Debye-type) spectral densities, can be found in Appendix C of ref 15. In order to obtain the motional parameters, a wide range of values of τ_R, N, and ϵ_{nonsec} were used to calculate a range of *B* and *C* values. τ_R is the mean rotational correlation time obtained from the geometric mean of the diffusion coefficients $R_\perp$ and $R_\parallel$ [$\tau_R^{-1} = 6(R_\parallel R_\perp)^{1/2}$], N is the ratio of $R_\parallel$ to $R_\perp$, and ϵ_{nonsec} is an adjustable parameter introduced into the spectral densities for nonsecular frequencies in the manner described by Hwang et al.[15] ϵ is related to the finite lifetime of the fluctuating torques causing the reorientation of the probe molecule.[15,17] The effects of ϵ_{nonsec}, though significant in the isotropic phase where $\tau_R^2\omega^2 \approx 1$, become less prominent in the ordered phases where the motion is slower and the nonsecular contributions to the spectral densities are smaller.

Our results are summarized in Table II. As has been typically noted for PD-Tempone in a variety of solvents[15,16a] (and as expected for a quasi-spherical solute), N is noted to lie between 1 and 1.2 in all phases of the solvent, indicating isotropic diffusion. In the isotropic phase of 6OCB–8OCB, the value of ϵ_{nonsec} was 4.9 ± 0.3, implying $\tau_R \approx \tau_M$, where τ_M represents the characteristic decay time associated with the fluctuating torques.[15]

The dependence of the mean rotational correlation time (τ_R) on temperature is shown in Figure 11, along with the activation energies for rotational diffusion indicated in parentheses (in kilocalories per mole). The reduction in ΔE_{act} in going from the isotropic to the nematic phase probably indicates that PD-Tempone is pushed toward the aliphatic tails of the liquid crystal molecules, an observation consistent with earlier studies of PD-Tempone in a similar liquid crystal, 8CB,[16a] and consistent with our comments in the text above.

TABLE II: Ordering and Dynamics of PD-Tempone in 6OCB–8OCB

phase	T, °C	$\langle D_{00}^2 \rangle$	$\langle D_{02}^2 + D_{0-2}^2 \rangle$	τ_R, ps	N	ΔE_{act}, kcal/mol
I	94.4			19.0	1.2	12.6
	91.3			23.0		
	88.5			25.5		
	84.7			35.5		
	81.9			36.5		
N	77.1	0.088	0.015	32.6	1.0	6.2
	75.6	0.100	0.021	33.7		
	72.6	0.104	0.025	36.5		
	68.0	0.106	0.028	41.2		
	63.1	0.110	0.030	47.0		
	55.9	0.122	0.039	57.7		
	50.7	0.130	0.041	66.8		
	47.2	0.136	0.042	74.2		
S_A	43.1	0.144	0.048	96.6	1.0	8.60
	40.1	0.150	0.050	109.5		
	38.5	0.153	0.050	117.2		
	35.5	0.157	0.050	133.4		
	33.1	0.160	0.049	148.2		
RN	31.7	0.164	0.050	160.2	1.0	9.10
	28.8	0.167	0.052	184.9		
	25.9	0.170	0.053	214.0		
	24.5	0.175	0.054	230.0		

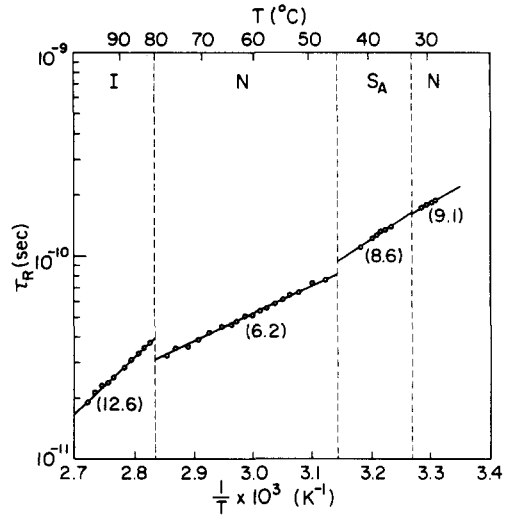

Figure 11. Rotational correlation times (τ_R) and activation energies (in parentheses; kcal/mol) for PD-Tempone in 6OCB–8OCB.

In the S_A phase, the activation energy (8.6 kcal/mol) increases relative to the nematic phase, which is again behavior similar to that observed for PD-Tempone in 8CB.[16a] This may suggest a little more access to the aromatic core region once ordered smectic layers form. As the temperature is lowered even further, the reentrant nematic phase is formed with very little change observed in the nature of the rotational dynamics of PD-Tempone.

(*ii*) *MOTA.* As with PD-Tempone, the spectra in all phases fall in the motional narrowing regime. It is of interest to compare our results obtained with MOTA with those from PD-Tempone.

The line-width parameters *B* and *C* in the various phases are shown in Figure 12. On comparing with Figure 10, we note some interesting features:

(i) The variation in *B* and *C* with temperature is over a much wider range for MOTA than for PD-Tempone in spite of the higher degree of ordering for the latter.

(ii) In any given phase, *B* is greater than *C* for MOTA; for PD-Tempone, except at very high temperatures, *B* is less than *C*. Furthermore, the separation between *B* and *C* is much greater for MOTA than for PD-Tempone.

(29) Rao, K. V. S.; Hwang, J. S.; Freed, J. H. *Phys. Rev. Lett.* **1976**, *37*, 515.

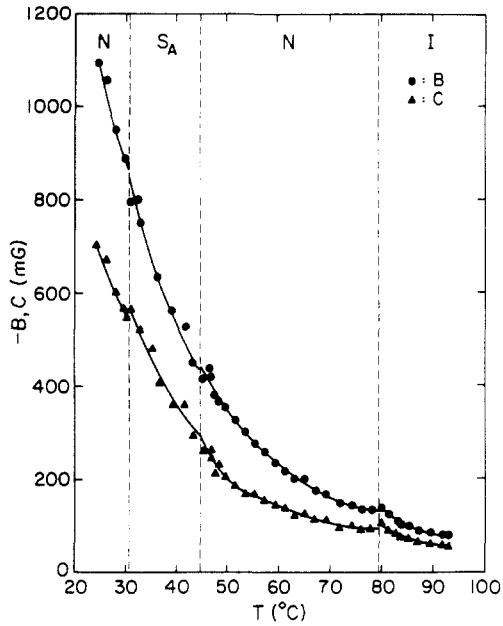

Figure 12. Line-width data (B and C) for MOTA in 6OCB–8OCB as a function of temperature.

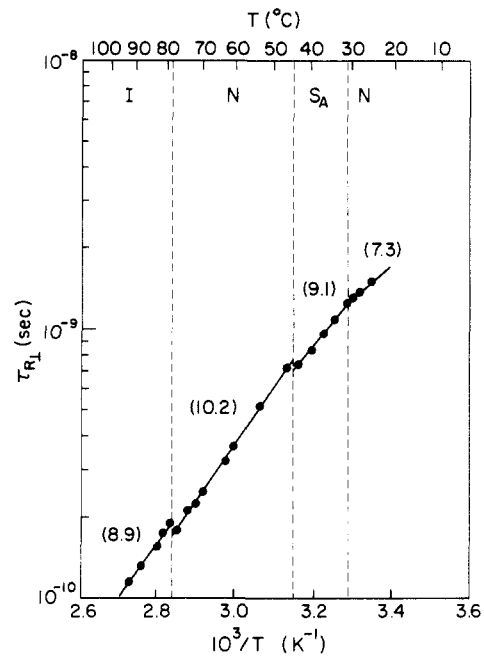

Figure 13. Rotational correlation times ($\tau_{R_\perp}$) and activation energies (in parentheses; kcal/mol) for MOTA in 6OCB–8OCB. The changes in N in the nematic phase are shown in Table III.

(iii) Though not obvious from the figures (owing to the different choice of scales), the critical divergences in the parameters are more prominent for MOTA than for PD-Tempone. However, with the former probe, no divergence was observed at the nematic side of the N–I transition.[26]

We shall discuss the significance of (i) and (ii) here. (iii) is discussed elsewhere in the context of critical effects.[26]

In the absence of critical effects, the parameters B and C depend upon (a) the anisotropy of the magnetic tensors in the diffusion frame, (b) the order parameters, and (c) the rotational correlation time (via the spectral densities). The ratio of B to C being greater than unity for MOTA and less than unity for PD-Tempone is a consequence of the difference in the ordering of the magnetic tensors in the diffusion frame: x''' for MOTA and y''' for PD-Tempone. The larger values for B and C in MOTA (compared with PD-Tempone) are indicative of slower motion, and their variation over a wider range (together with a variation in the ratio B/C from one phase to another) is consistent with the motion being anisotropic, the anisotropy parameter depending on the mesophase.

In Figure 13, we show plots of $\tau_{R_\perp}$ (where by definition, $\tau_{R_\perp}^{-1} = 6R_\perp$, $\tau_{R_\parallel}^{-1} = 6R_\parallel$, and $\tau_R = (\tau_{R_\perp}\tau_{R_\parallel})^{1/2}$) versus $1/T$. The simulation parameters are tabulated in Table III. In sharp contrast to PD-Tempone, the anisotropy ratio N for MOTA was noted to vary considerably within the nematic phase, changing from about 4 near the N–I transition to 27 near the N–S_A transition. This indicates not only that $R_\perp$ and $R_\parallel$ have different activation energies but also (as seen from Table III) that while $R_\perp$ progressively decreases as the temperature is lowered (motion becomes slower), $R_\parallel$ actually *increases* with decreasing temperature! Such behavior was not noted in the other phases. Such an increase in $R_\parallel$ is usually taken as implying an additional mode (or modes) of motion coupled to the reorientational motion (cf. ref 14–18). Although such behavior is not clearly understood in the present case, it is not inconsistent with the hypothesis that as the temperature is lowered, more voids are created within the hydrocarbon regions thereby lowering the steric resistance to internal motion (about the principal axis) in MOTA about the amide moiety. However, the larger than expected activation energy for overall reorientation (i.e., $\tau_{R_\perp}$) for a probe located mainly in the hydrocarbon regions (e.g., compare with P probe discussed in text below) may indicate additional steric inhibitions to rotational motions in directions perpendicular to the ordering axis of the molecule.

Though the motion is slower than PD-Tempone, the variation of τ_R is over 1 decade as with PD-Tempone (see Figure 10). We note that in the I, N, and S_A phases, the activation energy for overall reorientation (indicated in parentheses in kilocalories per mole) does not change very significantly. Given that the ordering of the probe is low and that it probably resides amidst the alkyl chains, this is not greatly surprising. Although in the reentrant nematic phase we find a decrease in ΔE_{act} (7.3 kcal/mol), the narrow width of the phase (about 7 °C) does not permit as good an assessment of ΔE_{act} as in the other phases. The large anisotropy parameter (N = 7–9) in all phases, the y''' ordering, and the larger activation energies for MOTA than for PD-Tempone in the ordered phases account for the overall higher sensitivity of the line-width parameters to temperature seen in MOTA.

TABLE III: Ordering and Dynamics of MOTA in 6OCB–8OCB

phase	T, °C	$\langle D_{00}^2 \rangle$	$\tau_{R_\perp}$, ns	N	$\Delta E_{act}(\tau_{R_\perp})$, kcal/mol
I	92.9		0.118	5	8.9
	87.9		0.139		
	85.0		0.154		
	83.2		0.164		
	80.5		0.180		
N	78.2	0.048	0.169	3.9	10.3
	74.1	0.063	0.202	5.0	
	71.9	0.069	0.221	5.6	
	69.2	0.071	0.249	6.6	
	64.0	0.081	0.314	9.1	
	60.2	0.085	0.375	11.6	
	53.5	0.090	0.516	17.9	
	47.3	0.093	0.700	27.1	
S_A	43.0	0.084	0.739	7	9.1
	40.6	0.085	0.827		
	36.6	0.084	0.968		
	32.7	0.086	1.120		
	30.8	0.089	1.318		
RN	29.5	0.087	1.341	9	7.3
	28.1	0.090	1.440		
	25.4	0.081	1.602		

(*iii*) *P-Probe.* ESR studies on liquid crystals using the P-probe have been carried out in these laboratories and are described in ref 18. Compared with PD-Tempone, P is a long and flexible molecule and more closely resembles a liquid crystal (Figure 2). Owing to its larger size, its overall motion is slower and one can indeed take advantage of this fact to study the model dependence, particularly in the lower temperature well-ordered phases.

Since the rotational correlation times for the P-probe in the ordered phases as obtained by line-shape simulations were found

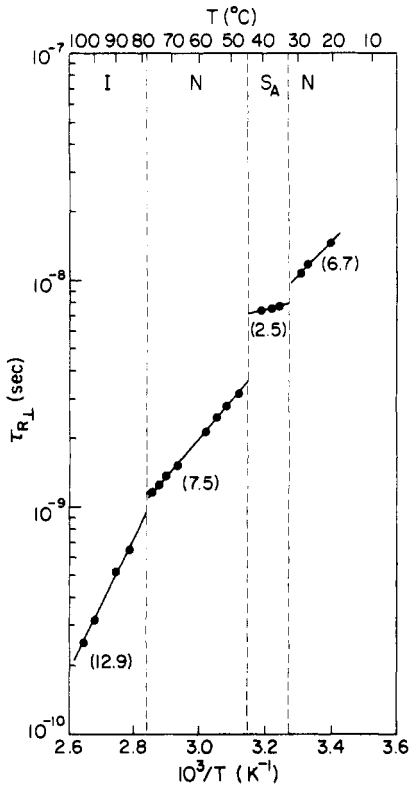

Figure 14. Rotational correlation times ($\tau_{R_\perp}$) and activation energies (in parentheses; kcal/mol) for P in 6OCB–8OCB.

to lie in the slow-motional regime, the line-width coefficients B and C are inappropriate parameters for describing the probe dynamics as they no longer relate simply to rotational correlation times.[17] Instead, line-shape simulations were performed. The dynamic parameters for the various mesophases are tabulated in Table IV. The variation of $\tau_{R_\perp}$ for the P-probe (Figure 14) covers a wider range than PD-Tempone or MOTA. In the isotropic phase, the activation energy of 12.9 kcal/mol is about the same as what we observed with PD-Tempone. However, the $\tau_{R_\perp}$ values are 1 order of magnitude smaller than those for PD-tempone, as is typical for this larger probe.[18] From our simulations, an anisotropy parameter of about 4 was obtained, consistent with the elongated shape of P. [For a prolate ellipsoid, an N of about 4 was estimated[15,18] with a long axis dimension of $r_{x'''} \approx 10$ Å,

TABLE IV: Ordering and Dynamics of P in 6OCB–8OCB

phase	T, °C	$\langle D_{00}^2 \rangle$	$\tau_{R_\perp}$, ns	N	ΔE_{act}, kcal/mol
I	104.2		0.26	4	12.9
	99.8		0.32		
	90.8		0.51		
	84.8		0.66		
N	77.0	0.186	1.20	10	7.5
	74.1	0.220	1.30		
	71.2	0.232	1.42		
	66.5	0.244	1.58		
	58.7	0.267	2.09		
	54.3	0.289	2.53		
	51.1	0.312	2.85		
	47.3	0.323	3.10		
S_A	40.5	0.301	7.36	15	2.5
	38.6	0.289	7.55		
	36.2	0.289	7.75		
RN	30.3	0.244	11.61	11	6.7
	27.7	0.244	12.50		
	23.0	0.267	15.26		

corresponding to half the length of the fully extended molecule and the short axes with dimensions of $r_{y'''} \approx r_{z'''} \approx 2.85$ Å for the piperidine ring.] In ref 18, the possible contribution of internal rotation of the piperidine ring was implied by an $N = 7$ for P in 4O,6 and an $N \approx 6$ for P in S2.

In the nematic phase, $\tau_{R_\perp}$ increases and the anisotropy parameter N increases to 10 (Table IV). This is because $R_\perp$ has increased by about 15%, while $R_\parallel$ has increased by 50%. Also, the activation energy in the nematic phase drops to 7.5 ± 0.3 kcal/mol. These observations are similar to those for P in 4O,6.[18] The reduced activation energy could imply location of the nitroxide moiety near the aliphatic chain with the large N, suggesting a significant contribution from the internal rotation of the piperidine ring.

In Figure 15a, we present some temperature- and angular-dependent spectra taken in the S_A phase, along with our simulations. Meirovitch et al.[18] found that their simulations for P in 4O,6 and S2 were best when a two-parameter ordering potential was used, whereas a one-parameter potential (λ only) was satisfactory for 5CB. Our observations in the present work are consistent with the need for only one ordering parameter.

On passing into the smectic phase, there is a very significant drop in the activation energy (2.5 kcal/mol). Such a decrease in ΔE_{act}, which was also noted to occur with P in S2, is interpreted in terms of the probe getting expelled from the rigid core regions of the smectic layer to the more fluid hydrocarbon regions. The

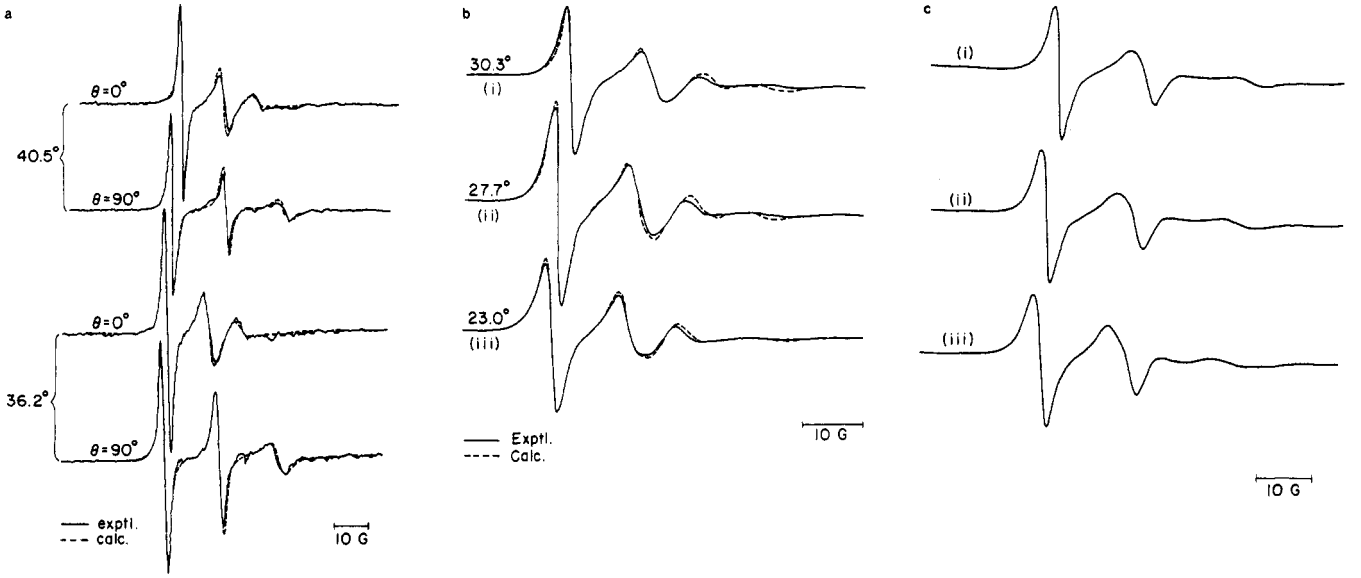

Figure 15. Experimental (solid lines) and simulated (broken lines) ESR spectra for P in 6OCB–8OCB in the (a) smectic-A and (b) reentrant nematic phases at temperatures as indicated. In a, the spectra were taken at 0° and 90° orientations of the smectic director with respect to the magnetic field. (c) Calculation performed assuming a cooperative distortion model for the reentrant nematic phase (see text). In all calculations, simulation parameters given in Tables I and IV were used.

value of 2.5 kcal/mol, however, is even lower than that seen with PD-Tempone. This may be due to the fact that PD-Tempone, on account of its smaller size, can partially experience the aromatic cores whereas the P-probe cannot. Consistent with expulsion of the P-probe molecules into the hydrocarbon regions, we observe a gradual decrease in its ordering in the smectic phase relative to the nematic phase. Also, N is noted to increase to 15, indicating an increased hindrance to rotational motion for P about its short axis.

When the temperature is lowered even further, the reentrant nematic phase is formed. ΔE_{act} increases to nearly its value for the higher temperature nematic phase, while N decreases to nearly its value for the nematic phase. Thus, the P-probe appears to exhibit rather similar dynamic behavior in the N and RN phases except for the higher viscosity at the lower temperatures in the RN phase (on account of which $\tau_{R_\perp}$ increases). However, the ordering of the P probe drops somewhat in the RN phase, becoming comparable to the values observed at higher temperatures in the nematic phase.

Finally, we compare our results from P in the S_A phases of 6OCB–8OCB and S2.[18] The spectra from S2 showed some unusual features: At low temperatures, the ESR spectra spread over a wide range in magetic field and additional peaks, that were not present in the nematic phase, begin to appear. These features were interpreted in terms of a cooperative chain distortion mechanism. The probes are located within the hydrocarbon chain region of the aligned bilayers. The effect of a local distortion in the chains is transmitted along the bilayer in the form of a coherent wave. The observed additional peaks in the spectra are believed to arise from contributions due to different orientations that the probe, embedded in the hydrocarbon matrix, makes with the magnetic field. The effects of this distortion were found to be most prominent at the lower temperatures (20 °C and below), and spectra taken at the higher temperatures did not show these unusual features. On the other hand, our spectra in the S_A phase of 6OCB–8OCB did not show these multiple lines and could be successfully simulated with a single value of θ, this being the angle that the mean director makes with the static field. The reason for this difference may be that, for S2, the additional peaks were observed for those temperatures where the probe was more highly ordered in the smectic phase ($\langle P_2 \rangle \approx 0.55$–$0.8$ in S2, whereas $\langle P_2 \rangle \approx 0.3$ in 6OCB–8OCB). Therefore, the spectra of P in the S_A phase of 6OCB–8OCB are not very sensitive to cooperative effects (e.g., compare the predictions of Figure 15b,c). Whether or not such chain distortion effects are occurring in 6OCB–8OCB solvent, there are striking similarities with S2 solvent in (i) the very low activation energy and (ii) the value of τ_R for comparable temperatures and phases. However, a much larger value of N is obtained for 6OCB–8OCB ($N = 15$) as compared to S2 ($N = 4$).

The spectra of P in the reentrant nematic phase of 6OCB–8OCB (≈24–30 °C) were indicative of overall slower motion, higher activation energy, and slightly decreased ordering relative to the S_A phase (Figure 15b and Table IV). This is consistent with the idea that, at densities exceeding the optimum, voids created as a consequence of bilayering tend to get filled. Thus, the P-probe experiences a more motionally restricted environment.

V. Discussion

A. Solute Behavior and the Reentrant Nematic. The ESR studies with the three spin labels (PD-Tempone, MOTA, and P-probe) in 6OCB–8OCB suggest that as smectic bilayers begin to form, the probes are expelled toward the hydrocarbon regions. The ability on the part of the probes to experience the more highly ordered and motionally restricted regions in the liquid crystal solvent (i.e., the aromatic cores) decreases in the order PD-Tempone > MOTA > P-probe, consistent with the increasing size of the molecules. This effect is reflected most dramatically in the observed dynamics of the P-probe, whose size should permit its accommodation in voids in the hydrocarbon regions in the S_A phase but should inhibit its presence in the vicinity of the cores. Consequently, its activation energy dramatically decreases in the S_A phase, and at the same time, its ordering decreases relative to the nematic phase. On the assumption that PD-Tempone and MOTA can still partially experience the cores in the S_A phase, while P can only experience the chain regions, it follows that when the transformation to the RN phase occurs, the change in the activation energy is greatest for the P-probe (its value in the RN phase being almost equal to that in the nematic phase), while the activation energies for PD-Tempone and MOTA in the S_A and RN phases are seen to be rather similar. Furthermore, if the observations with P in the S_A phase of 6OCB–8OCB are taken to reflect the dynamic molecular structure of the hydrocarbon regions of the smectic bilayer, then the ordering of P in the S_A and RN phases, which remains low and does not show the increase with decreasing temperature observed in the S_A phase of S2 (which also exhibits a bilayered S_A phase but no reentrant nematic), may imply that substantial chain disorder is consistent with the S_A–RN transition. That is, random chain packing is favored over well-aligned packing, and this favors the RN phase. Such a failure of chain alignment at the low temperatures would imply the greater importance of intermolecular interactions as the density is increased with decreasing temperature in driving the S_A–RN phase transition. The stronger intermolecular forces (and torques) are indicated by a doubling of τ_R on going from the S_A to the RN phase, as well as the increased activation energy.

In actual fact, the results from ^{2}H NMR on chain orientational order in reentrant nematics[12] show that all positions on the chain show gradually increasing orientational ordering (more precisely, increasing quadrupolar splittings) as the temperature is lowered through the S_A and RN phases with a typical flexibility gradient along the chain (except for the absence of an alternation along the chain). The end-chain region remains generally weakly ordered [$\langle P_2 \rangle \approx 0.07$–$0.15$ for methylene carbons 7 and 8 in 8OCB; see ref 12]. Thus, either the P-probe is further expelled to less ordered regions as overall ordering increases (but P-probe is almost as long as 6OCB) or nearby chains are rather disordered in the sense that they show little or no instantaneous local ordering beyond the observed mean ordering: i.e., random packing beyond the constraints of the weak mean ordering. This latter possibility is consistent with the absence of cooperative modes of chain motion and our inability to detect such effects in the ESR spectra of P-probe in 6OCB–8OCB, whereas they appear in the case of P-probe in the S_A phase of S2 and the nematic phase of 5CB. That is, in the latter cases, the ESR spectra show a distribution of directors with high order ($\langle P_2 \rangle \geq 0.5$) that is frozen on the ESR time scale but could be partially averaged on the NMR time scale.

To press this conjecture further would be to expect that, in a "normal" smectic, as T decreases (or density increases), the chains exhibit substantial short-range instantaneous order beyond the mean order observed in an NMR experiment. In the smectic phase of a "reentrant nematic", such short-range order is suppressed by a tendency toward more random positional order in the chain region, e.g., by the interpenetration of chains from adjacent bilayers (which tends to fill voids; cf. Figure 3). This makes the smectic phase of the reentrant nematic somewhat more like that of the nematic phase, at least with regard to the packing of different chains. Thus, in a normal smectic, collective packing of chains helps to stabilize the smectic phase (e.g., the decrease in entropy offsets an increase in the magnitude of the attractive (i.e., negative) internal energy). But, in a reentrant nematic, collective packing of chains is frustrated.

It appears to us that the elements of such a model are consistent with the optimum density phenomenological model of Prost and Pershan[9] as well as the molecular model of Dowell.[24] Also, there is perhaps a formal connection between our viewpoint of reentrance and one proposed by Prost and Barois[23] for explaining the multiplicity of smectic phases often observed in polar liquid crystals. These authors have shown that if the smectic free energy is expanded in terms of the mass density wave $\rho(\mathbf{q})$, then minima may occur for both $q = 2\pi/\alpha l$ and $q = 2\pi/l$, where α lies between 1 and 2. The former value of q, which corresponds to a partial bilayer smectic phase, is favored entropically since the loose packing of the chains allows for relatively unrestricted motion.

As the temperature is lowered, however, the contribution of this entropy term in lowering the free energy decreases, thus making the free energies corresponding to the semibilayer ($\alpha \approx 2$) and monolayer ($\alpha = 1$) comparable. In this situation, fluctuations into the monolayer phase destroy the bilayer arrangement.

B. Comparison with Other Results. We shall now compare the results from our ESR experiments with other experimental results on reentrant nematics.

Dong et al.,[30] who have studied the variation in the rotational diffusion constants $R_\perp$ and $R_\parallel$ with temperature for 26 wt % perdeuterated 6OCB–8OCB using ^{2}H-NMR, note the following: (i) N decreases from 240 near the N–I transition to about 30 in the RN phase. (ii) the activation energy associated with motion about the long axes ($R_\parallel$) remains practically unchanged at 11.4 kcal/mol in the N and S_A phases but increases slightly in the RN phase. (iii) Meanwhile, the activation energy for $R_\perp$ roughly doubles in value across the phase transitions (2.6, 4.8, and 11.0 kcal/mol for N, S_A, and RN phases, respectively). These results were taken to imply that the greater effective packing of the molecules in the reentrant nematic phase (due to pairing) inhibits the flipping of the molecules about their short axes—resulting in an increased activation energy for $R_\perp$.

However, our results on the rotational activation energies for the three spin probes show that although the rotational correlation times progressively increase in the order I–N–S_A–RN, the activation energies do not show any such trend. Even though the narrow temperature range of the reentrant nematic state precludes an analysis of the dynamics as reliable as that in the N and S_A phases, it is generally noted that ΔE_{act} for the RN phase is not very different from N (P-probe) or S_A (PD-Tempone and MOTA). Our results with PD-Tempone and MOTA indicate that the packing forces in the RN and S_A phases are similar, whereas the larger and more well-ordered P-probe shows that the reentrant nematic state is very similar to the nematic state.

Our results, although consistent with the idea that packing and molecular association could play an important role in affecting reentrance, are not consistent with saturation in pair formation being a necessary precursor to reentrance. The Arrhenius nature of the probe dynamics is consistent with a single activation energy (except for MOTA). Therefore, any changes in the dimer/monomer ratio with temperature must be continuous. This implies that any changes in structure that the liquid crystal molecules must undergo are much too delicate to exhibit appreciable effects on our spin probes and certainly not of the order that would account for dramatic changes in activation energy and the anisotropy parameter across all the phase transitions such as those observed by Dong.[30]

A conclusion similar to ours in regard to pairing (i.e., that a saturation is probably *not* the mechanism that drives reentrance) was reached by Kortan et al.,[13b] who showed that, in several 6OCB–8OCB mixtures, the mean molecular spacings and positional correlations in the N, S_A, and RN phases are closely similar to those on materials exhibiting a single-layer S_A phase (e.g., the *n*O,*m* compounds such as 4O,7.)[31] Furthermore, the liquid structure factor was the same in all the mesophases, thus arguing against any dramatic structural changes (e.g., pairing). An additional argument against any sudden changes in pairing is that the dielectric permittivity in 6OCB–8OCB varies smoothly across the transitions,[32] contrary to what would be expected if the pairing reached saturation (resulting in a significant change in the polarity and hence dielectric properties of the system). Our results on the activation energies, taken together with the X-ray and dielectric measurements, do not lend support to the view that reentrance occurs following a saturation in pair formation. Instead, Kortan et al.[13] speculate on the relevance of models involving competition between monolayer and bilayer formation (see above text).

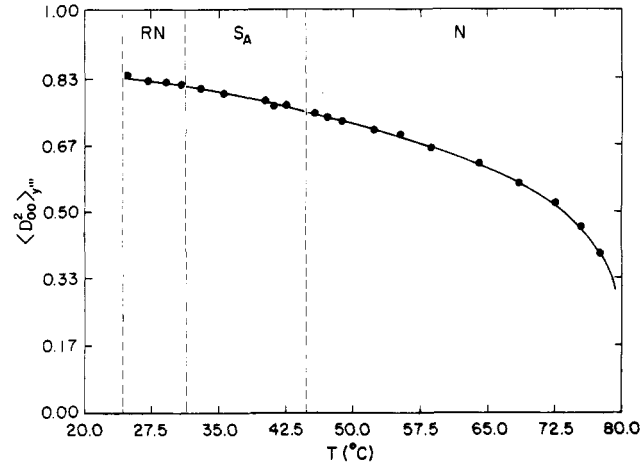

Figure 16. Ordering of CSL spin label in 6OCB–8OCB as measured from hyperfine splittings.

Finally, we briefly compare our observations with some typical results from magnetic resonance experiments of other investigators, where primary focus was placed on the changes in molecular ordering of solutes (and not their dynamics) at the N–S_A–RN transitions.[10,33] Thus, for example, ESR experiments on a mixture of CBOOA and HBAB performed by Luckhurst et al.[10] using two different probe molecules, one of which (CSL) probes the aromatic cores and the other of which (an alkyl chain nitroxide) probes the alkyl chains, show that (i) the orientational order near the cores is practically unaffected at the S_A–RN transition (increasing smoothly but gently through N–S_A–RN), while (ii) the alkyl chain probe shows no increase in ordering in the S_A phase, a result similar to our observation with the P-probe. We have also studied CSL in 6OCB–8OCB. It showed results similar to those with PD-Tempone, though with higher ordering and slower motion. In Figure 16, we show the dependence of CSL ordering with temperature (CSL orders with the magnetic y'''-axis approximately along the diffusion z'-axis). Our results on the ordering of CSL in the S_A and RN phases are virtually identical with the results of Luckhurst et al. in CBOOA–HBAB, i.e., a gradual increase in $\langle P_2 \rangle$ from about 0.7 to >0.8 as the temperature is lowered. (Also, in an ESR study of CSL in S2 by Meirovitch and Freed,[27] the authors find that the probe shows moderately high ordering ($S \approx 0.6$–0.7) and slow motion and tends to reside among the rigid cores in the smectic phase.) Thus, our results with CSL, as well as those of Luckhurst et al.,[10] show that the ordering of the aromatic cores proceeds in a fashion that shows little, if any, sensitivity to the various phase transitions (i.e., N–S_A–RN).

VI. Conclusions

The properties of reentrant nematics, as compared with liquid crystals that do not exhibit nematic reentrance (normal smectics), can be best appreciated when the results from our ESR studies on 6OCB–8OCB are compared with those using the same probes in liquid crystals composed of cyanobiphenyls, e.g., 8CB[16a] or S2[18a] (neither of which show reentrant phases). The comparisons are summarized below:

(i) In both cases (reentrant and nonreentrant liquid crystals), the probes behave very similarly in their dynamic properties; they get expelled toward the alkyl chains as smectic layers begin to form. PD-Tempone and MOTA, though mainly in the chain regions, can however partially experience the aromatic cores, while the P probe is completely buried in the chains.

(ii) The orientational ordering of the aromatic cores increases gradually through the N, S_A, and RN phases in a fashion that is not sensitive to these phase transitions. This is monitored by the CSL probe, which shows typically high ordering ($\langle P_2 \rangle \approx$ 0.7–0.8). Such results are basically the same for reentrant and nonreentrant liquid crystals.

(30) Dong, R. Y.; Richards, G. M.; Lewis, J. S.; Tomchuk, E.; Bock, E. *Mol. Cryst. Liq. Cryst.* **1987**, *144*, 33.
(31) (a) Garland, C. W.; Meichle, M.; Ocko, B. M.; Kortan, A. R.; Safinya, C. R.; Yu, L. J.; Litster, J. D.; Birgeneau, R. J. *Phys. Rev. A* **1983**, *27*, 3234. (b) Ocko, B. M.; Kortan, A. R.; Birgeneau, R. J.; Goodby, J. W. *J. Phys. (Les Ulis, Fr.)* **1984**, *45*, 113.
(32) Ratna, B. R.; Shashidhar, R.; Bock, M.; Gobl-Wunsch, A.; Heppke, G. *Mol. Cryst. Liq. Cryst.* **1983**, *99*, 285.
(33) Vaz, N. A. P.; Yaniv, Z.; Doane, J. W. *Chem. Phys. Lett.* **1983**, *98*, 354.

(iii) Results on the ordering and dynamics of P probe in the reentrant nematic liquid crystal suggest that the chains are more disordered in the S_A and RN phases (in the sense of chain packing) compared to the S_A phase of a normal smectic, whereas they experience enhanced resistance to rotational motion in the RN phase, probably due to enhanced packing in the chain region. This is suggestive of reduced short-range chain cooperativity in ordering and dynamics as increased packing of chains from adjacent layers occurs concomittent with the loss of smectic order.

(iv) In general, the nematic and S_A phases in systems exhibiting reentrance are rather similar to those in structurally similar liquid crystals where reentrance is not observed. At the molecular level, the N-S_A and S_A-RN transitions are very similar and the effects driving the transition are very subtle. Small changes in molecular properties can make a difference, e.g., the decrease in average chain length by the addition of 6OCB to 8OCB to produce a reentrant nematic. Previous X-ray[13] and density[20] results also demonstrate the similarities of these phase transitions with nothing dramatic occurring.

Registry No. 6OCB, 41424-11-7; 8OCB, 52364-73-5; PD-Tempone, 36763-53-8; MOTA, 14691-89-5; P, 64120-21-4; CSL, 121575-16-4.

NMR Studies of Rotational Motion at Low Viscosity

R. F. Evilia, J. M. Robert,† and S. L. Whittenburg*

Department of Chemistry, University of New Orleans, New Orleans, Louisiana 70148
(Received: September 26, 1988; In Final Form: April 7, 1989)

We have measured the rotational correlation time of dilute solutions of several small molecules dissolved in supercritical fluids using ^{14}N NMR spectroscopy. In supercritical fluids at the densities employed, the solubility is sufficiently high to obtain rapid acquisition of the spectra, while the viscosity is extremely small. Comparison of the rotational correlation times with the literature values obtained from light-scattering measurements at higher viscosity demonstrates that the Stokes-Einstein-Debye plot deviates from linearity as the inertial limit is approached. The measured correlation times compare favorably with the free-rotor correlation time.

Introduction

Many studies of rotational motion have demonstrated the general applicability of the Stokes-Einstein-Debye equation[1]

$$\tau = A\eta/T + \tau^\circ \quad (1)$$

where τ is the effective rotational correlation time whose definition for nonspherical molecules requires analysis of anisotropic reorientation, η is the solution viscosity, and T is the absolute temperature. A is the slope of the Stokes-Einstein-Debye plot, and τ° is the intercept. A and τ° are relatively insensitive to temperature and pressure.[2] The Stokes-Einstein-Debye equation is one form of Walden's rule that states that the correlation time is proportional to η/T.[3] While there is an overwhelming number of studies that demonstrate the validity of the Stokes-Einstein-Debye equation, there have been several studies that show deviations from this relationship.[4]

The physical interpretation of the A parameter is fairly well understood. It is related to the shape and volume of the rotating particle and the boundary condition for interaction between the interacting particle and the adjacent solvent. The Stokes-Einstein-Debye hydrodynamic theory models the particle as a sphere and assumes a continuum solvent.[5] This theory predicts that the A parameter is given by $A = V/[k_B l(l+1)]$, where l is the order of the rotational correlation function, V is the molecular volume, and k_B is Boltzmann's constant. The order of the rotational correlation function is equal to 2 for light-scattering and NMR spectroscopy. Perrin has removed the assumption of sphericity and enabled the theory to be applied to ellipsoidal particles.[6] Youngren and Acrivos have further extended the approach by incorporating molecules of arbitrary shape.[7] In their approach, the A parameter can be calculated from the three primary axial lengths and remains a function of the molecular volume. The Stokes-Einstein-Debye theory assumes stick boundary conditions; that is, the solvent adjacent to the rotating particle sticks to the particle. Hu and Zwanzig have extended the model to incorporate slip boundary conditions.[8] Thus, it is now possible to model the rotation of molecules of arbitrary shape in solution in the limits of stick and slip boundary conditions. For most small molecular fluids, slip boundary conditions are in good agreement with the experimental slopes,[9] while several examples of nonslip boundary conditions have been measured.[10]

The physical meaning of the intercept term in eq 1, τ°, is less clear. It can be obtained in two ways: By one method, it can be obtained by extrapolation of the Stokes-Einstein-Debye plot obtained from measurements carried out as a function of temperature. In this approach, the measurements are performed at high solvent viscosity and the data are extrapolated to $\eta/T \rightarrow 0$. Thus, the intercept is not related to the inertial limit, that is, to the free-rotor correlation time. Indeed, experiments have reported negative intercepts.[2,3,11] Kivelson and Evans have derived expressions that relate the τ° term to cross-correlation functions between torquelike terms and kinetic variables.[12] The other method for obtaining the intercept is to measure the rotational correlation time as a function of viscosity at sufficiently low

† Present address: Department of Chemistry, Hartwick College, Oneonta, NY 13820.

(1) Berne, B. J.; Pecora, R. *Dynamic Light Scattering*; Wiley: New York, 1976.
(2) Wolfe, M.; Jonas, J. *J. Chem. Phys.* **1979**, *71*, 3252. Herring, F. G.; Phillips, P. S. *J. Chem. Phys.* **1980**, *73*, 2603.
(3) Dote, J. L.; Kivelson, D.; Schwartz, R. N. *J. Phys. Chem.* **1981**, *85*, 2169.
(4) Kivelson, D.; Madden, P. A. *Annu. Rev. Phys. Chem.* **1980**, *31*, 523.
(5) Debye, P. *Polar Molecules*; Dover: New York, 1929.
(6) Perrin, F. *J. Phys. Radium* **1934**, *5*, 497.
(7) Youngren, G.; Acrivos, A. *J. Chem. Phys.* **1975**, *63*, 3846; *J. Fluid Mech.* **1975**, *69*, 377.
(8) Hu, C.; Zwanzig, R. *J. Chem. Phys.* **1970**, *52*, 6353.
(9) Cheung, C. K.; Jones, D. R.; Wang, C. H. *J. Chem. Phys.* **1976**, *64*, 3576.
(10) Higashigaki, Y.; Whittenburg, S. L.; Wang, C. H. *J. Chem. Phys.* **1978**, *69*, 3297. Whittenburg, S. L.; Wang, C. H. *J. Chem. Phys.* **1979**, *70*, 2035.
(11) Fury, M.; Jonas, J. *J. Chem. Phys.* **1976**, *65*, 2206. Patterson, G. D.; Lindsey, C. P.; Alms, G. R. *J. Chem. Phys.* **1978**, *69*, 3250.
(12) Evans, G. T.; Kivelson, D. *J. Chem. Phys.* **1986**, *84*, 385.

0022-3654/89/2093-6550$01.50/0